2018-07-05

Mechanistic Studies of [AlCp*]4 Combustion

Tang, Xin; DeLisio, Jeffery B.; Alnemrat, Suan; Hicks, Zachary; Stevens, Lauren; Stoltz, Chad A.; Hooper, Joseph P.; Eichhorn, Bryan W.; Zachariah, Michael R.; Bowen, Kit H....

ACS Publications

Tang, Xin, et al. "Mechanistic Studies of [AlCp*] 4 Combustion." Inorganic chemistry 57.14 (2018): 8181-8188.
http://hdl.handle.net/10945/65692

Inorganic Chemistry
Cite This: Inorg. Chem. 2018, 57, 8181−8188
Article
pubs.acs.org/IC

Mechanistic Studies of $[AlCp^*]_4$ Combustion

Xin Tang,[†,⊥] Jeffery B. DeLisio,[‡,⊥] Sufian Alnemrat,[§,⊥] Zachary Hicks,[†] Lauren Stevens,[‡] Chad A. Stoltz,[∥] Joseph P. Hooper,[*,§] Bryan W. Eichhorn,[*,‡] Michael R. Zachariah,[*,‡] Kit H. Bowen,[*,†] and Dennis H. Mayo[*,‡,∥]

[†]Department of Chemistry, Johns Hopkins University, Baltimore, Maryland 21218, United States
[‡]Department of Chemistry and Biochemistry, University of Maryland—College Park, College Park, Maryland 20742, United States
[§]Department of Physics, Naval Postgraduate School, Monterey, California 93943, United States
[∥]Research Department, Naval Surface Warfare Center Indian Head EOD Tech Division, Indian Head, Maryland 20640, United States

Supporting Information

ABSTRACT: The combustion mechanism of $[AlCp^*]_4$ (Cp* = pentamethylcyclopentadienyl), a ligated aluminum(I) cluster, was studied by a combination of experimental and theoretical methods. Two complementary experimental methods, temperature-programmed reaction and T-jump time-of-flight mass spectrometry, were used to investigate the decomposition behaviors of $[AlCp^*]_4$ in both anaerobic and oxidative environments, revealing AlCp* and Al_2OCp^* to be the major decomposition products. The observed product distribution and reaction pathways are consistent with the prediction from molecular dynamics simulations and static density functional theory calculations. These studies demonstrated that experiment and theory can indeed serve as complementary and predictive means to study the combustion behaviors of ligated aluminum clusters and may help in engineering stable compounds as candidates for rocket propellants.

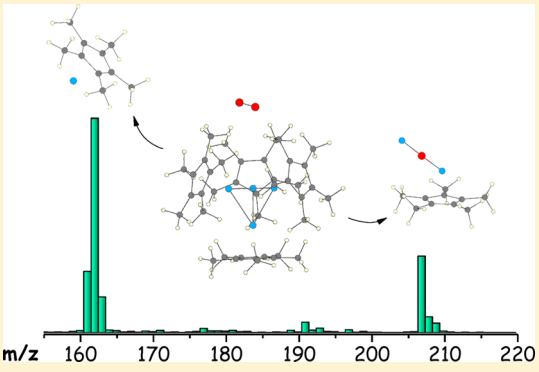

INTRODUCTION

The need for high-energy-density ingredients for propulsion applications has driven research into new propellants, fuels, and oxidizers. While there have been significant advances in energetic materials, energy gains, especially from traditional carbon, hydrogen, nitrogen, and oxygen (CHNO) architectures, have been increasingly marginal. Metal-based systems, however, have very high volumetric heats of combustion relative to traditional CHNO ingredients, showing high potential for use as a fuel, fuel additive, or ingredient. Aluminum metal is a particularly attractive fuel in that and it is abundant and possess a high energy density. However, aluminum's ever-present 2−3 nm thick Al_2O_3 oxide shell retards oxygen transport to the Al core, which slows the release of its thermochemical energy. Aluminum nanoparticles have high surface to mass ratios, potentially allowing for significant gains relative to the bulk material. However, as surface areas increase, the mass fraction of the Al_2O_3 shell increases (lowering energy content) and slow oxidation kinetics due to hindered oxygen transport remains an impediment to fast combustion rates.[1] In addition, particle sintering during combustion limits the benefits of the nanostructured particles.[2]

A potential solution is the use of molecular clusters of aluminum in low oxidation states—a class of compounds known as metalloid aluminum clusters.[3] These compounds typically contain aluminum in low formal oxidation states (≤+2.0) with the larger clusters containing metallic cores of near closest packed aluminum atoms. All of the clusters are surrounded by stabilizing ligands, which prevent the formation of an oxide shell.[3] Therefore, they are potentially useful fuels due to their inherently small sizes and the presence of highly reactive aluminum without an Al_2O_3 shell. While many aluminum clusters have been synthesized and structurally characterized, little experimental data have been reported describing their combustion behavior.

To better understand the oxidative chemistry of the low-oxidation-state Al atoms and their attendant ligands in a cluster compound, we have investigated the simplest low-oxidation-state Al cluster, $[AlCp^*]_4$ (Cp* = pentamethylcyclopentadienyl) (**1**).[4] The complex is characterized by a tetrahedral cluster of metal−metal-bonded Al(I) atoms each coordinated by an η^5-Cp* ligand. Unlike the larger metalloid clusters that require a cocondensation reactor for preparation,[3] **1** can be prepared through standard solution chemistry, such as salt metathesis of aluminum monochloride,[4a] alkali-metal reduction of $AlCp^*Cl_2$,[4b] and most recently via reductive elimination of Cp^*H from $AlCp^*_2H$.[4a,d] It has also been used as a starting

Received: March 8, 2018
Published: July 5, 2018

DOI: 10.1021/acs.inorgchem.8b00589
Inorg. Chem. 2018, 57, 8181−8188

material in the preparation of bimetallic complexes as well as intermetallic nanoparticles.[5]

The solution chemistry of **1** has been extensively studied.[4e,6,4a,e,6,4b,7,8] Several oxidation reactions with **1** have been investigated that include oxidative addition of chalcogens to give $[AlCp^*E]_4$ (E = O, S, Se, Te) heterocubanes containing fully oxidized Al(III) ions[4b,7] and reactions with oxygen and water to form oxo- and hydroxo-bridged aluminum(III) compounds.[8] In addition to the solution phase, the reactivity and structure of **1** in the gas phase have been studied via Fourier transform ion cyclotron resonance mass spectrometry (FT-ICR) by the Schnöckel group.[9] However, the heterogeneous oxidation of **1** with either solid-state or gas-phase oxidizers has not been evaluated and such information is central to understanding the role of Al clusters as solid-state fuels. Specifically, the question of whether the Al core or the organic ligand shell will react sequentially or simultaneously with gas-phase oxidizers has not been addressed and has a direct effect on the kinetics of combustion.

Theoretical studies on low-oxidation-state aluminum clusters have been carried out for nearly as long as the compounds themselves have been reported. Early reports on experimental solution dynamics of **1** tracked by ^{27}Al NMR relied heavily on density functional theory (DFT) calculations for support.[4e] More recently, theoretical investigations into the heats of combustion,[10] oxidative reaction chemistry,[11] and solution dynamics[12] of a variety of low-oxidation-state aluminum cluster materials have been reported. Our studies[11b] have predicted that initial reactions occur between molecular oxygen and the metallic aluminum cluster core, rather than oxidation of the ligand shell. This behavior is consistent with the reported solution and solid-state reaction chemistry of related reduced aluminum compounds.[13] The predicted reactivity is advantageous from an energetic applications standpoint; namely, the more energetic oxidation of the metallic aluminum core precedes the combustion of the external organic ligand shell.[4b,7,8] We recently have demonstrated that oxidation of $[AlBrNEt_3]_4$, which has an inorganic ligand sphere (Al is coordinated by N and Br atoms), gives AlO in the presence of gas-phase oxygen transfer reagents.[13]

Herein we report a multifaceted mechanistic study of $[AlCp^*]_4$ oxidation by molecular oxygen. An oxidation pathway predicted by molecular dynamics is presented, along with the observation of predicted intermediates in both temperature-programmed reaction (TPR) and T-jump time-of-flight mass spectrometry (TOF-MS) experiments. In addition, details regarding the preparation and T-jump spectra of two $[AlCp^*]_4$/oxidizer mixtures are presented.

EXPERIMENTAL METHODS

Materials. The tetrameric Al(I) cluster $[AlCp^*]_4$ (**1**) samples were prepared via literature procedures and verified via single-crystal X-ray diffraction prior to use.[4b,d] Bismuth oxide (Bi_2O_3) nanopowder was purchased from Sigma-Aldrich. Potassium periodate (KIO_4) nanoparticles were prepared by dissolving KIO_4 (Sigma-Aldrich) in distilled water and then spray-dried using a previously described aerosol-based procedure.[14] Hexane was dried over sodium benzophenone ketyl and stored over activated 3 Å molecular sieves.

Temperature-Programmed Reaction. A TPR setup implemented with a Hiden HAL/3F PIC quadrupole mass spectrometer (QMS) was used to characterize the reactivity of $[AlCp^*]_4$. A home-built vacuum suitcase was employed to introduce **1** to an ultrahigh-vacuum (UHV) environment. The suitcase has a special differentially pumped double-sealed design, which ensures an oxygen-free environment during the transfer process and also enables rotational/translational motion of the sample in vacuo. The schematic of the home-built vacuum suitcase is shown in Figure S1 in the Supporting Information, and details of the UHV analytic setup can be found elsewhere.[15] A piece of fresh-cut sodium was added as a sacrificial oxygen getter during the transfer process. A small amount (~2 mg) of **1** was loaded onto a tantalum sample plate (affixed to the plate with carbon tape) in a glovebox and subsequently transferred to a UHV analytic chamber by the aforementioned vacuum suitcase. The sample was heated by a tungsten filament behind the sample, and the temperature of the sample was monitored by a K-type thermocouple attached to the sample holder. A temperature ramping rate of 0.65 °C/s was used. The reaction products that desorbed from the surface were measured by QMS with a glass shroud in front of the ionizer. To characterize the reactivity of the $[AlCp^*]_4$ with oxygen, and to differentiate between reactions with residual O_2/H_2O in the chamber and during the transfer, isotopically labeled oxygen ($^{18}O_2$) was dosed through a leak valve (1×10^5 Torr) to react with $[AlCp^*]_4$.

T-jump TOF-MS. A previously described T-jump TOF-MS coupled with an air-sensitive sample holder (ASSH, see Figure S2) was used for time-resolved speciation analysis at high heating rates.[13,14,16] Samples were prepared in a glovebox with 2 mg of combined solids suspended in 1 mL of dry hexane. Samples containing **1** and Bi_2O_3 or KIO_4 (1:3 cluster to oxidizer ratio by mass) were suspended in hexane and mixed via sonication for 10 min in a sealed, oxygen-free vial. Samples were loaded as a suspension in hexanes via autopipette onto 76 μm platinum (Pt) wires held by the ASSH within the glovebox. Oxidized $[AlCp^*]_4$ samples were prepared by loading the sample onto the Pt wires within the glovebox and then exposing the dry material to air prior to insertion into the TOF-MS.

To ensure air-free transfer, the roughing chamber of the TOF-MS was pumped and purged with UHP nitrogen (N_2) gas prior to mounting the ASSH and a positive pressure of N_2 was maintained in the roughing chamber during mounting of the ASSH. Once the ASSH was inserted into the instrument under vacuum, the platinum wires were resistively heated at rates as high as 5×10^5 °C/s within the TOF-MS (sampling rate 10 kHz) with time-resolved wire temperatures calculated using the Callendar–Van Dusen equation. A 600 MHz digital oscilloscope was used for data acquisition. To perform activation energy analysis, wire heating rates were varied by increasing or decreasing the pulse width and/or driving voltage of the heating circuit.

THEORETICAL METHODS

Molecular Dynamics. Molecular dynamics calculations were performed using a Car–Parrinello method as implemented in the CPMD code.[17] Electronic exchange and correlation effects were treated with the PBE functional.[18] Interactions between the nuclei and electrons were described with Vanderbilt ultrasoft pseudopotentials and a plane wave basis set with 25 Ry cutoff energy. Simulations were performed in the NVT ensemble with Nose–Hoover thermostats and a thermostat frequency of 2600 cm^{-1}. A fictitious mass of 400 amu was used, allowing a time step of 4 au (~0.097 fs) for the integration of equations of motion. Nonperiodic boundary conditions were used in the Poisson solver for all calculations. Simulations were performed at 2000 K (~1727 °C).

Static Calculations. All static DFT calculations were performed using the Gaussian09 package[19] with the M06-2X functional and 6-31G* basis set.[20] This functional/basis set combination successfully predicts very accurate thermodynamics for three known experimental tetramerization enthalpies.[12] The optimized structures at the M06-2X/6-31G* level were used to calculate the harmonic frequencies, which were then scaled by a factor of 0.947 on the basis of prior calibrated frequency scaling.

RESULTS

Temperature-Programmed Reaction. Figure 1 presents the TPR spectra of pure $[AlCp^*]_4$ from 35 to 210 °C with a ramping rate of 0.65 °C/s without an oxidant present. The

DOI: 10.1021/acs.inorgchem.8b00589
Inorg. Chem. 2018, 57, 8181–8188

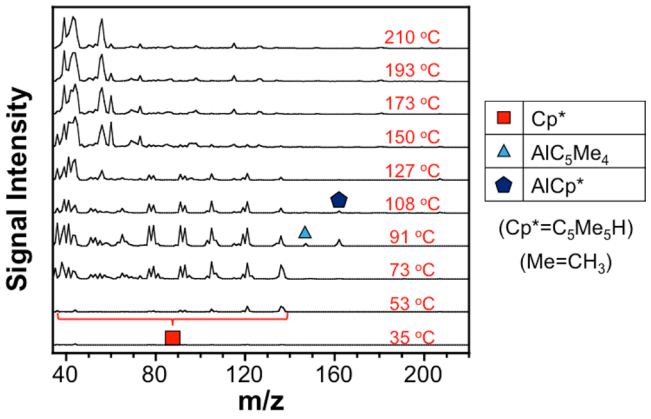

Figure 1. TPR spectra of $[AlCp^*]_4$ from 35 to 210 °C with a ramping rate of 0.65 °C/s.

major peaks of the desorption products are assigned by referring to a previous mass spectroscopic study on pentamethylcyclopentadiene (Cp*H).[21] The mass spectra of $[AlCp^*]_4$ contain a parent peak of Cp*H at 136 amu, with the lower mass peaks corresponding to the major fragments of Cp*H (121, 105, 93, and 79 amu). In addition to the fragments from Cp*H, a mass peak at 162 amu emerges as the sample temperature is raised. We assign this peak to AlCp*, which is predicted by previous calculations to be a major thermal decomposition product of aluminum−cyclopentadienyl clusters.[10] The peak at 147 amu is attributed to AlC_5Me_4, a fragment of AlCp* formed by the loss of one methyl group.

Figure 2 presents the TPR spectra of the products generated from the reaction between solid $[AlCp^*]_4$ and $^{18}O_2$ (1×10^{-5} Torr) between 36 and 213 °C, with a ramping rate of 0.65 °C/s. In addition to the fragments of Cp* and the AlCp* unit, a higher mass peak at 207 amu is also observed as the sample temperature is increased. We attribute this peak at 207 amu to $Al_2{}^{18}OCp^*$, formed from the oxidation of $[AlCp^*]_4$.

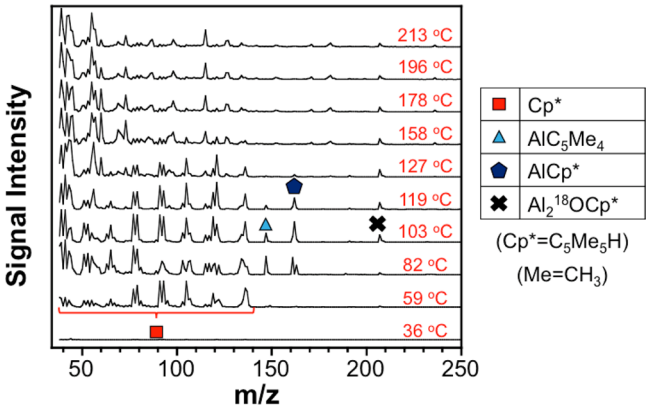

Figure 2. TPR spectra of $[AlCp^*]_4$ in 1×10^{-5} Torr of $^{18}O_2$ from 36 to 213 °C with a ramping rate of 0.65 °C/s.

T-jump TOF-MS. A suite of air-free T-jump TOF-MS experiments was performed on $[AlCp^*]_4$. The data collected via TOF-MS are time-resolved, allowing for temporal analysis of individual m/z signal intensities in addition to full spectral data at a given time. To compare spectra between different experiments, all spectra are normalized to their respective maximum atomic aluminum signal intensity (m/z 27). It should be noted that the electron impact ionization fragmentation patterns for Cp*H and for KCp* have very minor peaks at m/z 27, meaning that the signal intensity at m/z 27 in these experiments has a minor contribution from the fragmentation of the Cp*H.[21] The T-jump TOF-MS spectrum for KCp* is shown in Figure S3.

Figure 3a shows the anaerobic mass spectrum (MS) trace at the time of the maximum m/z 27 signal intensity. In addition to the labeled Cp* fragments, the AlCp* fragment (m/z 162) is also detected in the T-jump TOF-MS results (see Figure 3a).

In addition to anaerobic measurements, an $[AlCp^*]_4$ sample was dried on the wire, transferred anaerobically out of the glovebox, and exposed to air for 1 h prior to rapid heating to examine the postoxidation products. Figure 3b shows the MS at the time of the maximum m/z 27 signal intensity of the oxidized sample. This exposure mechanism provides a solid/gas oxidation mechanism akin to that of the TPR experiments described in the previous section. An increase in the m/z 18 and 43 fragments is observed relative to the anaerobic $[AlCp^*]_4$ sample, corresponding to H_2O and AlO, respectively. The AlCp* fragment at m/z 162 is not detected. Species corresponding to the fragmentation of Cp*H are minimal, but a new fragment, m/z 207, is detected.

To further investigate the species detected at m/z ~207, $[AlCp^*]_4$ was oxidized in three different oxidizing environments prior to heating: pure oxygen, air, and oxygen with a partial pressure of D_2O. Under each oxidizing atmosphere, the highest signal intensity peaks fall in the m/z 206−209 range corresponding to the Al_2OCp^* species with the addition of up to three hydrogens. Figure S4 shows the MS data from 520 to 860 °C in the m/z 205−215 range. There are significantly fewer species detected in the higher end of the range for the sample oxidized in pure oxygen, which we attribute to the lower number of available hydrogen atoms in the anhydrous pure oxygen environment.

Thermally Activated Reaction between $[AlCp^*]_4$ and Oxidizers. Bi_2O_3 and KIO_4 nanopowders were physically mixed with $[AlCp^*]_4$ (1/3 fuel/oxidizer mass ratio) to oxidize the cluster during rapid heating. In $[AlCp^*]_4/KIO_4$ mixtures, Al oxidation is observed upon heating; no noticeable decomposition occurs prior to thermal activation, even after 1 month of storage under a dry, inert atmosphere. Figure 4 shows temporal plots of m/z 27, 43, and 32 products of the pure cluster (A) and mixture with KIO_4 (B). The MS shows an increased m/z 43 peak corresponding to the formation of AlO, presumably due to Al oxidation by gas-phase oxygen released from the KIO_4. As seen in Figure 4B, oxygen release from the KIO_4 occurs slightly after the maximum Al signal intensity. A second Al and AlO peak is observed as the oxygen signal intensity increases at 1.7 ms.

The addition of Bi_2O_3 did not lead to observable oxidation of the cluster. We attribute the lack of oxidation to the temporal mismatch in oxygen release and gas-phase Al (or AlCp) formation in the T-jump experiment. Control T-jump studies on Bi_2O_3 show oxygen release above 900 °C (see Figure S5).[22] We have shown that oxidation of $[AlBr(NEt_3)]_4$ under similar conditions is maximized when oxygen evolution coincides with cluster vaporization and greatly diminished when the events are temporally shifted.[23,25] Similar results are observed for $[AlCp^*]_4/Bi_2O_3$ mixtures.

Activation Energy Calculations. To obtain an activation energy of $[AlCp^*]_4$ decomposition, heating rates were varied between ~1×10^5 and ~3.5×10^5 °C/s. The decomposition temperature is defined as the wire temperature at the point

DOI: 10.1021/acs.inorgchem.8b00589
Inorg. Chem. 2018, 57, 8181−8188

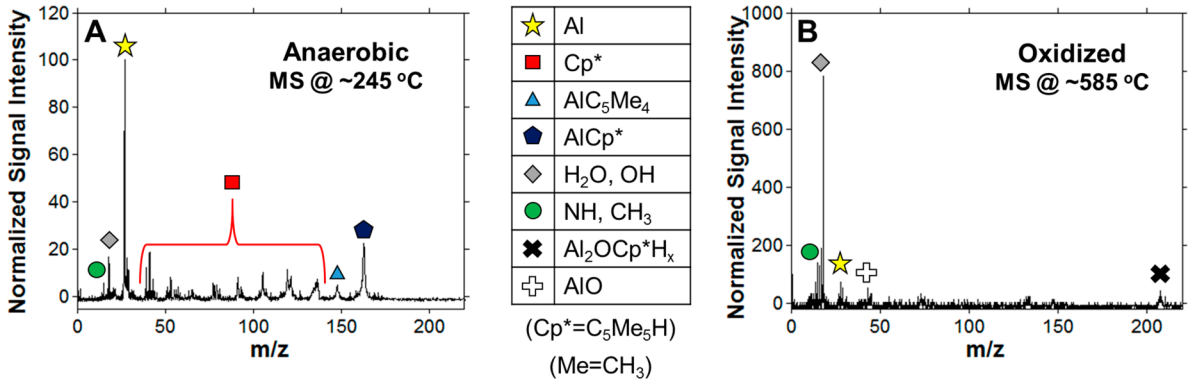

Figure 3. MS of anaerobic (A) and oxidized (B) $[AlCp^*]_4$ at wire temperatures of ~245 and ~585 °C, respectively, during T-jump experiments. Both samples were heated at a rate of ~2 × 10^5 °C/s, and spectra are normalized to their respective m/z 27 maximum signal intensity.

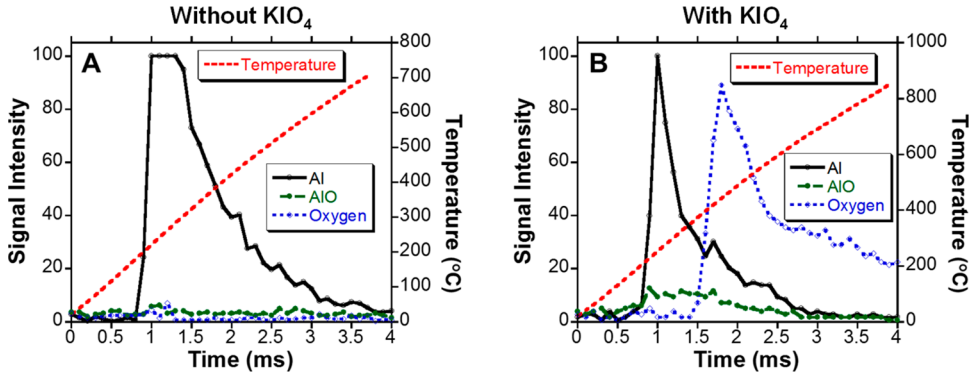

Figure 4. Temporal speciation for m/z 27, 32, and 43 of rapidly heated $[AlCp^*]_4$ (A) and $[AlCp^*]_4$ /KIO_4 (B). Both spectra are normalized to their respective maximum m/z 27 signal intensities.

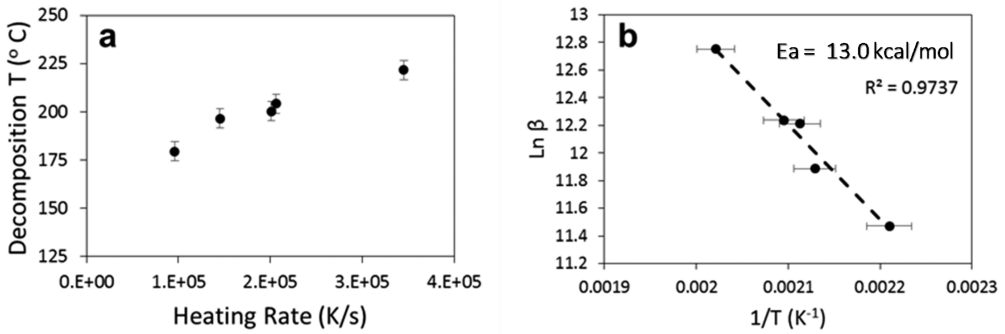

Figure 5. Decomposition temperature (first appearance of m/z 27) vs heating rate (A) and Arrhenius plot (B) of rapidly heated $[AlCp^*]_4$.

where m/z 27 is first detected, as seen in Figure 5a. Figure 5b shows the resulting Arrhenius plot of heating rate, β, vs the inverse of the decomposition temperature and yields an $[AlCp^*]_4$ activation energy for decomposition of 13.0 ± 0.3 kcal/mol. For comparison, the activation energy for decomposition of $[AlBr{\cdot}NEt_3]_4$ is 10.2 kcal/mol.[13]

Theoretical Results. We performed ab initio molecular dynamics (MD) simulations of the oxidation of $[AlCp^*]_4$ for comparison with the oxidation and decomposition products seen in the TPR and T-jump TOF-MS experiments. The starting point for the current simulation was our prior MD simulations of singlet O_2 interacting with the cluster.[20] Using a metadynamics algorithm to artificially accelerate the reaction, we observed a hindered crossing of the ligand steric barrier by the O_2, followed by oxygen splitting at the core. The aluminum/ligand bonds remained intact during the initial barrier crossing. Here we continue these simulations with ab initio MD to observe the subsequent decomposition products. No biasing potentials were used, but the simulations were run at a high computational temperature of 2000 K (~1727 °C) to accelerate chemical reactions. These temperatures are typical for this manner of simulation. After a very long simulation time (~400 ps), we arrive at final products that are consistent with those seen via TPR and T-jump TOF-MS.

The decomposition of the tetramer starting from the initial oxidized state was analyzed from the long trajectory and broken into the four major reaction steps given below. These states were then extracted from the trajectory, and their enthalpies of reaction were calculated using the M06-2X functional and 6-31G* basis set, a method known to give

DOI: 10.1021/acs.inorgchem.8b00589
Inorg. Chem. 2018, 57, 8181−8188

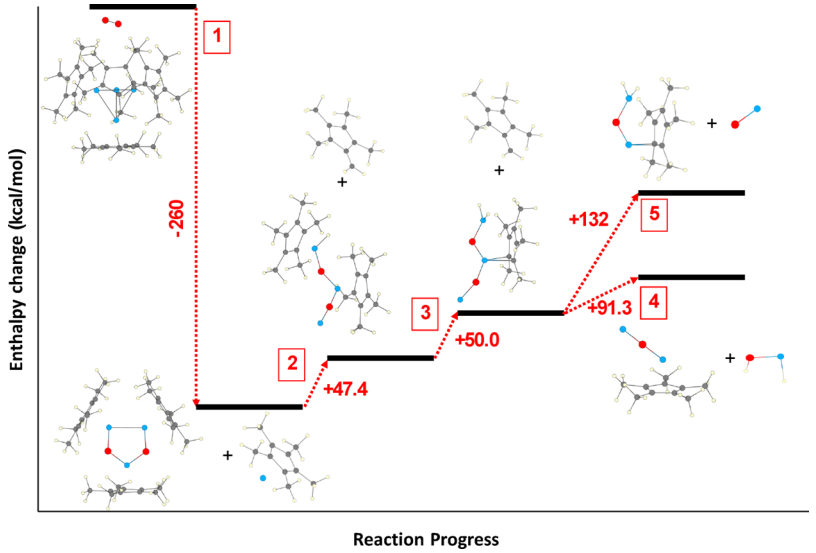

Figure 6. Schematic of the major steps in the calculated oxidation pathway of $[AlCp^*]_4$. The vertical scale corresponds to enthalpy changes in kcal/mol.

accurate tetramerization enthalpies for $[AlCp^*]_4$, $Al_4(C_5Me_4iPr)$, and $Al_4(C_5Me_4Pr)$ on the basis of comparison with previous experiments.[12]

The oxidation and decomposition of $Al_4Cp_4^*$ with a single O_2 molecule proceeds as follows. The initial configuration is shown in Figure 6. First, the O_2 moves across the ligand barrier, splits, and forms an $[(AlCp^*)_3O_2]$ cluster with a planar Al_3O_2 core. This initial step was studied in detail in our previous molecular dynamics simulations.[10] There, ab initio molecular dynamics combined with a metadynamics algorithm was used to show that O_2 reacts preferentially with the Al_4 core, moving through a transition state barrier of 10.8 kcal/mol that arises from ligand steric bulk and reorientation of the oxygen. A single AlCp* unit detaches following this process, and the overall reaction is exothermic (−260 kcal/mol). The resulting planar $Al_3O_2Cp^*_3$ complex, shown in step 1 in Figure 6, is stable over a very long MD simulation time (note that typical trajectories for ab initio MD are on the order of 10 ps or less). Approximately 70 ps after the initial reaction, a Cp* ligand transfers one H from a methyl group to a nearby Al atom in the core and the resultant tetramethylfulvene ligand then detaches from the complex (step 2). The enthalpy of this reaction is +47.4 kcal/mol. The same process is repeated from another Cp* ligand with approximately the same change in enthalpy (step 3). The resulting Y-shaped $Al_3O_2H_2Cp^*$ complex is very computationally stable; after an additional 50 ps of MD time, one of the two hydrogen atoms transfers to a nearby O and the system decomposes into the final products HAlOH and Al_2OCp^* with an enthalpy change of +91.3 kcal/mol (step 4). The HAlOH is likely to decompose further in the presence of other products; further decomposition has yet to be studied. Simulations were stopped at this point, as all major decomposition products (AlCp* and Al_2OCp^*) seen in the MD trajectory are also consistent with the TPR mass spectrometry experiments. Further examination of the intermediates led to an alternate final reaction step resulting in formation of $H_2AlOAlCp^*$ and AlO (step 5), which is calculated to have a larger enthalpy change than step 4 but is observed in the T-jump experiments.

The final reduced set of reaction steps is

1. $Al_4Cp^*_4 + O_2 \rightarrow Al_3O_2Cp^*_3 + AlCp^*$ | ΔH= −260 kcal/mol
2. $Al_3O_2Cp^*_3 \rightarrow Cp^*(-H) + Al_2O_2Al(+H)Cp^*_2$ | ΔH = +47.4 kcal/mol
3. $Al_2O_2Al(+H)Cp^*_2 \rightarrow Al_2O_2Al(+2H)Cp^* + Cp^*(-H)$ | ΔH = +50.0 kcal/mol
4. $Al_2O_2Al(+2H)Cp^* \rightarrow AlOAlCp^* + HAlOH$ | ΔH = +91.3 kcal/mol
5. $Al_2O_2Al(+2H)Cp^* \rightarrow H_2AlOAlCp^* + AlO$ | ΔH = +132 kcal/mol

DISCUSSION

The results presented in this study are complementary. The TPR results demonstrate the behavior of solid-state **1** while it is thermally ramped at a moderate heating rate. The observation of the AlCp* fragment (m/z 162) is in agreement with previously reported theoretical calculations and solution measurements, which show the Al−Al bonds to be weaker than Al−Cp* bonds. $[AlCp^*]_4$ has been purified by sublimation; the observation of monomeric AlCp* during a thermal ramp while under vacuum suggests mass transport of monomeric AlCp* during sublimation. In the presence of $^{18}O_2$, formation of oxygen-containing species is observed. Of particular note is the signal at m/z 207, corresponding to $[Cp^*Al_2{}^{18}O]^+$. This product also appears in the MD simulations (step 4, Figure 6); the stochastic simulation trajectory initially produced $[Cp^*Al_2O]$ upon thermal decomposition of $[Cp^*Al(OAl)\text{-}OAlH_2]$. The observation of a peak at elevated temperature at m/z 207 indicates the presence of $[Cp^*Al_2{}^{18}O]$.

Other fragments present in the TPR experiments are in good agreement with the EI fragmentation pattern of Cp*H and KCp*. The presence of Al, CO, and H_2O was not measured; O_2 present in the $[AlCp^*]_4/^{18}O_2$ experiment resulted in a spectral cutoff at m/z 37 to avoid saturation of the detector by $^{18}O_2$. As such, it is not possible to quantify the amount of atomic aluminum generated by thermal decomposition of $[AlCp^*]_4$ at low heating rates. The mass spectrum shows peaks indicative of Cp*H and AlCp*, products predicted by the computational trajectory of oxidation of $[AlCp^*]_4$ by O_2.

DOI: 10.1021/acs.inorgchem.8b00589
Inorg. Chem. 2018, 57, 8181−8188

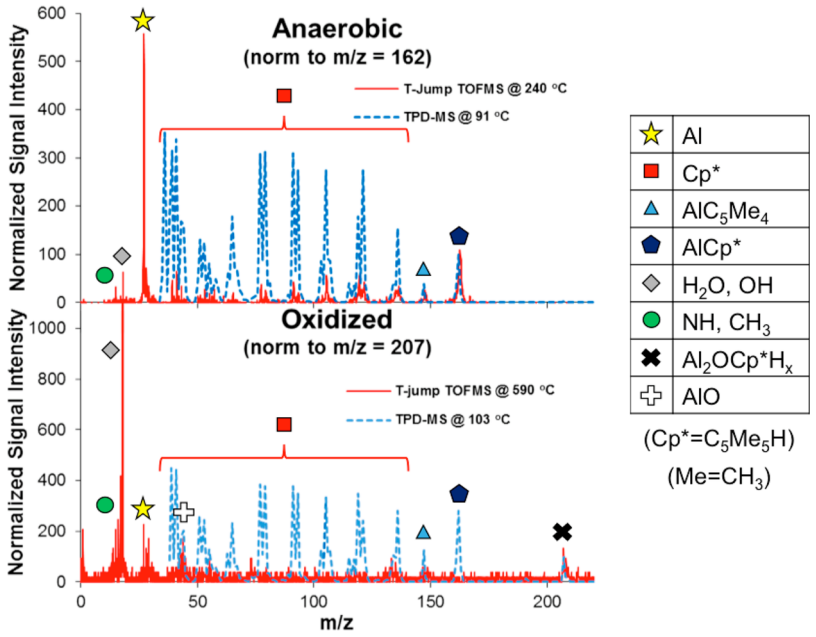

Figure 7. Overlaid normalized T-jump TOF-MS and TPR-MS results for heating of $[AlCp^*]_4$ in an anaerobic environment and in the presence of oxygen.

The anaerobic T-jump experiments provide decomposition behavior of $[AlCp^*]_4$ in a rapid heating environment. The experimental results show the generation of a large m/z 27 peak. This peak is readily assigned to atomic aluminum, as the m/z 27 contribution from fragmentation of Cp*H and KCp* is minimal. At the time of peak signal intensity, significant peaks are present for Al (m/z 27) and AlCp* (m/z 162). In addition to Al and AlCp*, peaks associated with the fragmentation of Cp*H are observed in the mass spectrum, though at relatively low signal intensity. Generally, the fragments observed in mass spectra of **1** generated by TPR and T-jump are similar, though the relative intensities of aluminum-containing fragments (Al and AlCp*) are higher in the T-jump experiments (see Figure 7). Data generated by both techniques are directly comparable, as ionization is achieved by electron impact in both methods.

To study the oxidation behavior of **1** in a combustive environment, physical mixtures of **1** with KIO_4 and Bi_2O_3 were prepared as suspensions in hexanes. Previous experiments have shown that the related Al(I) tetramer $[AlBrNEt_3]_4$ generates AlO upon heating with gas-phase oxygen transfer reagents (KIO_4) but not with solid-state oxidizers (Bi_2O_3). Similar results were observed in the case of **1**: the spectrum of a mixture of **1** and Bi_2O_3 shows no difference in fragmentation, while the mixture of **1** with KIO_4 results in formation of a moderate amount of AlO.

The mass spectra of samples of **1** oxidized by air showed minimal signals for Cp*H fragments; the main observed peaks are those of H_2O, Al, CO_2, and AlO. The lack of observed Cp*H signals is likely due to the volatility of liquid Cp*H formed during hydrolysis of **1**. When solid **1** is oxidized by air in the T-jump antechamber, a peak at m/z 207 is observed, corresponding to the kinetic product predicted in the MD simulations ($AlCp^*OAlH_2$, step 5, Figure 6). It is likely that this observed product is a result of the rapid heating of a partially oxidized $Cp^*_xAl_yO_z$ solid product.

Tetrameric $[AlCp^*]_4$ is relatively inert in the solid state and is reported to undergo slow oxidation by air and water.[4b] However, it is readily oxidized by N_2O and O_2 in solution,[7] and samples of $[AlCp^*]_4$ suspended in dry hexane form amorphous white powders immediately upon exposure to ambient atmosphere.

These results combine to show experimental evidence for the computationally predicted reaction pathway between $[AlCp^*]_4$ and O_2 (Figure 6). This reaction pathway—insertion of O_2 into the Al cluster core, followed by loss of AlCp* and then two stepwise hydrogen transfers from ligand to aluminum concurrent with loss of reduced ligand—results in an asymmetric Y-shaped intermediate that can eliminate to give two products observed under different reaction conditions. Under high heating rate T-jump conditions, the kinetic products (AlO + $H_2AlOAlCp^*$) are formed; under lower heating rate TPR conditions, the thermodynamic products ($HAlOH$ + $AlOAlCp^*$) are observed.

The results of the T-jump TOF-MS experiments highlight differences in product formation between $[AlCp^*]_4$ and the previously studied $[AlBr(NEt_3)]_4$. Upon exposure to ambient atmosphere, $[AlCp^*]_4$ loses significant signal intensity from Cp*H fragments, presumably due to the volatile nature of neutral Cp*H formed upon oxidation. In contrast, the fragmentation of NEt_3 was virtually unchanged during studies of anaerobically and aerobically prepared $[AlBr(NEt_3)]_4$, a result of formation of nonvolatile $HNEt_3Br$ during hydrolysis/oxidation of the aerobically prepared sample.[13] This study also provides an additional mixture of molecular aluminum fuel and strong oxidizer (KIO_4) that is stable as a suspension in dry hexane.

CONCLUSIONS

This study ties together two complementary experiments and demonstrates the utility of theory. Here, the experimental data show evidence of the predicted reaction pathway, validating the computational methods used. The ability to reliably predict the oxidation pathway of a small, relatively simple Al cluster system such as **1** is crucial in accurate simulations on larger systems; the reaction trajectory in this study took place over ~400 ps of MD time (and many months on a supercomputer).

DOI: 10.1021/acs.inorgchem.8b00589
Inorg. Chem. 2018, 57, 8181−8188

Further, validation of the theoretical code increases the likelihood of future success: future experimental studies will be supported by computational data, which has shown in this case to be predictive. Similarly, future computational studies may be designed to relate to experiment with the appropriate considerations. For these systems, experiment and theory can indeed serve as complementary methods and may help in engineering stable compounds for future use. Future studies will involve more complex systems and a combined theoretical/experimental approach.

■ ASSOCIATED CONTENT

Supporting Information

The Supporting Information is available free of charge on the ACS Publications website at DOI: 10.1021/acs.inorgchem.8b00589.

Details of experimental setups, TOF and MS spectra, and ignition temperatures (PDF)

■ AUTHOR INFORMATION

Corresponding Authors

*E-mail for J.P.H.: jphooper@nps.edu.
*E-mail for B.W.E.: eichhorn@umd.edu.
*E-mail for M.R.Z.: mrz@umd.edu.
*E-mail for K.H.B.: kbowen@jhu.edu.
*E-mail for D.H.M.: dennis.mayo@bep.gov.

ORCID

Xin Tang: 0000-0002-1896-2617
Joseph P. Hooper: 0000-0003-4899-1934
Michael R. Zachariah: 0000-0002-4115-3324
Kit H. Bowen: 0000-0002-2858-6352

Author Contributions

⊥X.T., J.B.D., and S.A. contributed equally to this work.

Notes

The authors declare no competing financial interest.

■ ACKNOWLEDGMENTS

This work was supported by the Defense Threat Reduction Agency (DTRA) under Grant No. HDTRA1-15-1-0031 and the Air Force Office of Scientific Research (AFOSR) under Grant No. FA9550-15-1-0259.

■ REFERENCES

(1) (a) Rai, A.; Park, K.; Zhou, L.; Zachariah, M. R. Understanding the mechanism of aluminium nanoparticle oxidation. *Combust. Theory Modell.* **2006**, *10* (5), 843−859. (b) Trunov, M. A.; Schoenitz, M.; Dreizin, E. L. Effect of polymorphic phase transformations in alumina layer on ignition of aluminium particles. *Combust. Theory Modell.* **2006**, *10* (4), 603−623. (c) Chowdhury, S.; Sullivan, K.; Piekiel, N.; Zhou, L.; Zachariah, M. R. Diffusive vs Explosive Reaction at the Nanoscale. *J. Phys. Chem. C* **2010**, *114* (20), 9191−9195. (d) Firmansyah, D. A.; Sullivan, K.; Lee, K.-S.; Kim, Y. H.; Zahaf, R.; Zachariah, M. R.; Lee, D. Microstructural Behavior of the Alumina Shell and Aluminum Core Before and After Melting of Aluminum Nanoparticles. *J. Phys. Chem. C* **2012**, *116* (1), 404−411. (e) Ermoline, A.; Dreizin, E. L. Equations for the Cabrera−Mott kinetics of oxidation for spherical nanoparticles. *Chem. Phys. Lett.* **2011**, *505* (1), 47−50. (f) Zhou, W.; DeLisio, J. B.; Wang, X.; Egan, G. C.; Zachariah, M. R. Evaluating free vs bound oxygen on ignition of nano-aluminum based energetics leads to a critical reaction rate criterion. *J. Appl. Phys.* **2015**, *118* (11), 114303.

(2) Egan, G. C.; Sullivan, K. T.; Olson, T. Y.; Han, T. Y.-J.; Worsley, M. A.; Zachariah, M. R. Ignition and Combustion Characteristics of Nanoaluminum with Copper Oxide Nanoparticles of Differing Oxidation State. *J. Phys. Chem. C* **2016**, *120* (51), 29023−29029.

(3) Schnöckel, H. Structures and Properties of Metalloid Al and Ga Clusters Open Our Eyes to the Diversity and Complexity of Fundamental Chemical and Physical Processes during Formation and Dissolution of Metals. *Chem. Rev.* **2010**, *110* (7), 4125−4163.

(4) (a) Dohmeier, C.; Robl, C.; Tacke, M.; Schnöckel, H. The Tetrameric Aluminum(I) Compound $[\{Al(\eta^5\text{-}C_5Me_5)\}_4]$. *Angew. Chem., Int. Ed. Engl.* **1991**, *30* (5), 564−565. (b) Schulz, S.; Roesky, H. W.; Koch, H. J.; Sheldrick, G. M.; Stalke, D.; Kuhn, A. A Simple Synthesis of $[(Cp^*Al)_4]$ and Its Conversion to the Heterocubanes $[(Cp^*AlSe)_4]$ and $[(Cp^*AlTe_4]$ ($Cp^*=\eta^5\text{-}C_5(CH_3)_5$). *Angew. Chem., Int. Ed. Engl.* **1993**, *32* (12), 1729−1731. (c) Sitzmann, H.; Lappert, M. F.; Dohmeier, C.; Uffing, C.; Schnöckel, H. Cyclopentadienyl derivatives of aluminum (I). *J. Organomet. Chem.* **1998**, *561* (1−2), 203−208. (d) Ganesamoorthy, C.; Loerke, S.; Gemel, C.; Jerabek, P.; Winter, M.; Frenking, G.; Fischer, R. A. Reductive elimination: a pathway to low-valent aluminium species. *Chem. Commun.* **2013**, *49* (28), 2858−2860. (e) Gauss, J.; Schneider, U.; Ahlrichs, R.; Dohmeier, C.; Schnöckel, H. ^{27}Al NMR Spectroscopic Investigation of Aluminum(I) Compounds - Ab initio Calculations and Experiment. *J. Am. Chem. Soc.* **1993**, *115* (6), 2402−2408.

(5) (a) Yu, Q.; Purath, A.; Donchev, A.; Schnöckel, H. The first structurally characterized coordination compound containing direct Al-Cr bonding: $Cp^*Al\text{-}Cr(CO)_5$. *J. Organomet. Chem.* **1999**, *584* (1), 94−97. (b) Ganesamoorthy, C.; Wessing, J.; Kroll, C.; Seidel, R. W.; Gemel, C.; Fischer, R. A. The Intermetalloid Cluster $[(Cp^*Al\text{-}Cu)_6H_4]$, Embedding a Cu_6 Core Inside an Octahedral Al_6 Shell: Molecular Models of Hume-Rothery Nanophases. *Angew. Chem., Int. Ed.* **2014**, *53* (30), 7943−7947. (c) Cokoja, M.; Parala, H.; Birkner, A.; Fischer, R. A.; Margeat, O.; Ciuculescu, D.; Amiens, C.; Chaudret, B.; Falqui, A.; Lecante, P. Organometallic Synthesis of β-CoAl Nanoparticles and β-CoAl/Al Nanoparticles and Their Behaviour upon Air Exposure. *Eur. J. Inorg. Chem.* **2010**, *2010*, 1599−1603.

(6) Huber, M.; Schnöckel, H. $Al_4(C_5Me_4H)_4$: Structure, reactivity and bonding. *Inorg. Chim. Acta* **2008**, *361* (2), 457−461.

(7) Stelzer, A. C.; Hrobarik, P.; Braun, T.; Kaupp, M.; Braun-Cula, B. Completing the Heterocubane Family $[Cp^*AlE]_4$ (E = O, S, Se, and Te) by Selective Oxygenation and Sulfuration of $[Cp^*Al]_4$: Density Functional Theory Calculations of $[Cp^*AlE]_4$ and Reactivity of $(Cp^*AlO]_4$ toward Hydrolysis. *Inorg. Chem.* **2016**, *55* (10), 4915−4923.

(8) Zhu, H. P.; Chai, J. F.; Jancik, V.; Roesky, H. W.; Merrill, W. A.; Power, P. P. The selective preparation of an aluminum oxide and its isomeric C-H-activated hydroxide. *J. Am. Chem. Soc.* **2005**, *127* (29), 10170−10171.

(9) (a) Koch, K.; Burgert, R.; Stösser, G.; Schnöckel, H. Understanding of the Structure, Bonding, Formation and Decomposition of Metalloid Aluminum Clusters—A Fourier Transform Ion Cyclotron Resonance Study of Solid AlCp*. *Eur. J. Mass Spectrom.* **2005**, *11* (5), 469−474. (b) Weiß, K.; Schnöckel, H. FT/ICR−mass spectrometry in nanotechnology: the investigation of metalloid clusters. *Anal. Bioanal. Chem.* **2003**, *377* (7), 1098−1101. (c) Koch, K.; Schnöckel, H. Structure and Reactivity of Al_2Cp^{*+} in the Gas Phase. Experiments on the Problematic Nature of the Aluminum-Aluminum-Multiple Bond. *Z. Naturforsch., B* **2004**, *59*, 1512.

(10) Williams, K. S.; Hooper, J. P. Structure, Thermodynamics, and Energy Content of Aluminum-Cyclopentadienyl Clusters. *J. Phys. Chem. A* **2011**, *115* (48), 14100−14109.

(11) (a) Alnemrat, S.; Hooper, J. P. Ab initio metadynamics simulations of oxygen/ligand interactions in organoaluminum clusters. *J. Chem. Phys.* **2014**, *141*, 144304. (b) Alnemrat, S.; Hooper, J. P. Oxidation of ligand-protected aluminum clusters: An ab initio molecular dynamics study. *J. Chem. Phys.* **2014**, *140*, 104313. (c) Alnemrat, S.; Hooper, J. P.; Vasiliev, I.; Kiefer, B. The role of equilibrium volume and magnetism on the stability of iron phases at high pressures. *J. Phys.: Condens. Matter* **2014**, *26* (4), 046001.

DOI: 10.1021/acs.inorgchem.8b00589
Inorg. Chem. 2018, 57, 8181−8188

(12) Tomlinson, W. W.; Mayo, D. H.; Wilson, R. M.; Hooper, J. P. The Role of Ligand Steric Bulk in New Monovalent Aluminum Compounds. *J. Phys. Chem. A* **2017**, *121* (24), 4678−4687.
(13) DeLisio, J. B.; Mayo, D. H.; Guerieri, P. M.; DeCarlo, S.; Ives, R.; Bowen, K.; Eichhorn, B. W.; Zachariah, M. R. Oxidation and decomposition mechanisms of air sensitive aluminum clusters at high heating rates. *Chem. Phys. Lett.* **2016**, *661*, 168−172.
(14) Jian, G. Q.; Feng, J. Y.; Jacob, R. J.; Egan, G. C.; Zachariah, M. R. Super-reactive Nanoenergetic Gas Generators Based on Periodate Salts. *Angew. Chem., Int. Ed.* **2013**, *52* (37), 9743−9746.
(15) (a) Tang, X.; Bumueller, D.; Lim, A.; Schneider, J.; Heiz, U.; Ganteför, G.; Fairbrother, D. H.; Bowen, K. H. Catalytic Dehydration of 2-Propanol by Size-Selected $(WO_3)_n$ and $(MoO_3)_n$ Metal Oxide Clusters. *J. Phys. Chem. C* **2014**, *118* (50), 29278−29286. (b) Tang, X.; Hicks, Z.; Ganteför, G.; Eichhorn, B. W.; Bowen, K. H. Adsorption and Decomposition of DMMP on Size-Selected $(WO_3)_3$ Clusters. *ChemistrySelect* **2018**, *3* (13), 3718−3721.
(16) (a) Zhou, L.; Piekiel, N.; Chowdhury, S.; Zachariah, M. R. T-Jump/time-of-flight mass spectrometry for time-resolved analysis of energetic materials. *Rapid Commun. Mass Spectrom.* **2009**, *23* (1), 194−202. (b) Zhou, L.; Piekiel, N.; Chowdhury, S.; Zachariah, M. R. Time-Resolved Mass Spectrometry of the Exothermic Reaction between Nanoaluminum and Metal Oxides: The Role of Oxygen Release. *J. Phys. Chem. C* **2010**, *114* (33), 14269−14275. (c) Piekiel, N. W.; Zhou, L.; Sullivan, K. T.; Chowdhury, S.; Egan, G. C.; Zachariah, M. R. Initiation and Reaction in Al/Bi_2O_3 Nanothermites: Evidence For The Predominance of Condensed Phase Chemistry. *Combust. Sci. Technol.* **2014**, *186* (9), 1209−1224.
(17) *CPMD version 3.17*; http://www.cpmd.org.
(18) Perdew, J. P.; Burke, K.; Ernzerhof, M. Generalized gradient approximation made simple. *Phys. Rev. Lett.* **1996**, *77* (18), 3865−3868.
(19) Frisch, M. J.; Trucks, G. W.; Schlegel, H. B.; Scuseria, G. E.; Robb, M. A.; Cheeseman, J. R.; Scalmani, G.; Barone, V.; Mennucci, B.; Petersson, G. A.; Nakatsuji, H.; Caricato, M.; Li, X.; Hratchian, H. P.; Izmaylov, A. F.; Bloino, J.; Zheng, G.; Sonnenberg, J. L.; Hada, M.; Ehara, M.; Toyota, K.; Fukuda, R.; Hasegawa, J.; Ishida, M.; Nakajima, T.; Honda, Y.; Kitao, O.; Nakai, H.; Vreven, T.; Montgomery, J. A.; Peralta, J. E.; Ogliaro, F.; Bearpark, M.; Heyd, J. J.; Brothers, E.; Kudin, K. N.; Staroverov, V. N.; Kobayashi, R.; Normand, J.; Raghavachari, K.; Rendell, A.; Burant, J. C.; Iyengar, S. S.; Tomasi, J.; Cossi, M.; Rega, N.; Millam, J. M.; Klene, M.; Knox, J. E.; Cross, J. B.; Bakken, V.; Adamo, C.; Jaramillo, J.; Gomperts, R.; Stratmann, R. E.; Yazyev, O.; Austin, A. J.; Cammi, R.; Pomelli, C.; Ochterski, J. W.; Martin, R. L.; Morokuma, K.; Zakrzewski, V. G.; Voth, G. A.; Salvador, P.; Dannenberg, J. J.; Dapprich, S.; Daniels, A. D.; Farkas; Foresman, J. B.; Ortiz, J. V.; Cioslowski, J.; Fox, D. J. *Gaussian 09, Revision B.01*; Gaussian Inc., Wallingford, CT, 2009.
(20) Hehre, W. J.; Ditchfield, R.; Pople, J. A. Self—Consistent Molecular Orbital Methods. XII. Further Extensions of Gaussian—Type Basis Sets for Use in Molecular Orbital Studies of Organic Molecules. *J. Chem. Phys.* **1972**, *56* (5), 2257−2261.
(21) National Institute of Standards and Technology (U.S.), NIST chemistry webbook. In *NIST standard reference database 69* [Online]; National Institute of Standards and Technology: Washington, D.C.; http://webbook.nistgov/chemistry/.
(22) Jian, G.; Chowdhury, S.; Sullivan, K.; Zachariah, M. R. Nanothermite reactions: Is gas phase oxygen generation from the oxygen carrier an essential prerequisite to ignition? *Combust. Flame* **2013**, *160* (2), 432−437.

DOI: 10.1021/acs.inorgchem.8b00589
Inorg. Chem. 2018, 57, 8181−8188